Proc. Natl. Acad. Sci. USA
Vol. 93, pp. 6247–6251, June 1996
Medical Sciences

Dynamic contrast-enhanced magnetic resonance imaging reveals stress-induced angiogenesis in MCF7 human breast tumors

(MCF7 cells/breast cancer/microcapillary permeability/gadolinium diethylenetriamine pentaacetic acid)

EDNA FURMAN-HARAN, RAANAN MARGALIT, DOV GROBGELD, AND HADASSA DEGANI*

Department of Chemical Physics, Weizmann Institute of Science, 76100 Rehovot, Israel

Communicated by Britton Chance, University of Pennsylvania, Philadelphia, PA, March 4, 1996 (received for review November 27, 1995)

ABSTRACT **The mechanism of contrast enhancement of tumors using magnetic resonance imaging was investigated in MCF7 human breast cancer implanted in nude mice. Dynamic contrast-enhanced images recorded at high spatial resolution were analyzed by an image analysis method based on a physiological model, which included the blood circulation, the tumor, the remaining tissues, and clearance via the kidneys. This analysis enabled us to map in rapidly enhancing regions within the tumor, the capillary permeability factor (capillary permeability times surface area per voxel volume) and the fraction of leakage space. Correlation of these maps with T_2-weighted spin echo images, with histopathology, and with immunohistochemical staining of endothelial cells demonstrated the presence of dense permeable microcapillaries in the tumor periphery and in intratumoral regions that surrounded necrotic loci. The high leakage from the intratumoral permeable capillaries indicated an induction of a specific angiogenic process associated with stress conditions that cause necrosis. This induction was augmented in tumors responding to tamoxifen treatment. Determination of the distribution and extent of this stress-induced angiogenic activity by contrast-enhanced MRI might be of diagnostic and of prognostic value.**

Angiogenesis and neovascularization play an important role in tumor growth and metastasis (1–3). Characterization of the vascular state of a tumor may facilitate development of novel strategies for cancer diagnosis and assessment of prognosis. Recently, numerous studies have shown a statistically significant correlation between increased intratumoral microvessel density and the risk of metastasis or decreased survival of patients with solid tumors of different origin (4–10). In breast cancer specifically, vascularization has been shown to be significantly higher in node-positive tumors than in node-negative tumors, and a high degree of vascularization was found to be associated with poorer prognosis (4–7). The microcirculation of growing tumors has many characteristics not found in the microcirculation of normal tissues. These characteristics include abnormal morphology, absence of vasomotion, increased fragility, and increased permeability (11, 12). The increased permeability gives rise to increased leakage of tracers including magnetic resonance imaging (MRI) contrast agents.

Contrast-enhanced MRI, primarily with gadolinium diethylenetriamine pentaacetic acid (GdDTPA) as a contrast agent, has been extensively used to diagnose tumors in almost all organs. In breast especially, contrast-enhanced MRI was found to be useful in accurately delineating breast lesions (13). Moreover, dynamic contrast-enhanced MRI demonstrated that the rate of change in signal enhancement is an important parameter for the distinction of breast masses (14).

Quantitative characterization of the time evolution of MRI contrast enhancement requires understanding of the underlying physiological and magnetic resonance mechanisms involved in the generation of enhancement curves. Furthermore, to overcome tumor heterogeneity, meaningful quantification requires imaging at high spatial resolution and voxel by voxel image analysis procedures. Despite recent attempts to provide a physiological/pharmacokinetic approach to contrast-enhanced data of tumors (15–20), including breast carcinoma (21, 22), the angiogenic processes and factors that determine the extent, time course, and spatial distribution of the enhancement are not fully understood.

To clarify the mechanism of contrast enhancement in breast tumors, we monitored at high spatial resolution the dynamic of GdDTPA enhancement in MCF7 human breast cancer implants in nude mice. These tumors have been extensively investigated in our laboratory during hormonal manipulation with estrogen and tamoxifen (23–27). Here we present a detailed image analysis of contrast-enhanced data, which enabled us to map in rapidly enhanced regions the capillary surface area times permeability and the cellularity of the tumors. Correlation of these maps with T_2-weighted images, with histological sections and with sections stained for endothelial cells sliced in the same plane as the MR images, revealed the presence of dense, highly permeable capillaries at the boundary of necrotic regions. The results have indicated that a unique angiogenic induction of permeable capillaries, in the vicinity of regions subjected to conditions that lead to cell death and necrosis, is responsible for intratumoral contrast enhancement. The demonstration of this induction by Gd-DTPA-enhanced MRI is consistent with previous findings that vascular endothelial growth factor, known also as vascular permeability factor (VEGF/VPF), is highly expressed around the periphery of necrotic cords of tumors (28, 29). Thus, stress-induced angiogenesis can be identified *in vivo* by dynamic contrast-enhanced MRI.

MATERIALS AND METHODS

MCF7 Tumors. MCF7 cells were cultured routinely under standard conditions and were prepared for inoculation as described elsewhere (23, 24). Approximately 10^7 cells were injected subcutaneously into the flank of each CD1-NU female, athymic mice, 6 to 8 weeks old. Before the injection, a pellet of 17-β-estradiol (0.72 mg per pellet, 60-day release time; Innovative Research of America, Sarasota, FL) was implanted underneath the back skin. Tumor growth was modulated by replacing the estradiol pellet with a tamoxifen pellet (5 mg per pellet, 45-day release time; Innovative Research of America, Sarasota, FL). All mice were anesthetized during the MRI measurement with sodium pentobarbital at a

The publication costs of this article were defrayed in part by page charge payment. This article must therefore be hereby marked "*advertisement*" in accordance with 18 U.S.C. §1734 solely to indicate this fact.

Abbreviations: GdDTPA, gadolinium diethylenetriamine pentaacetic acid; VEGF/VPF; vascular endothelial growth factor/vascular permeability factor; TE, echo time; TR, repetition time.

*To whom reprint requests should be addressed.

dose of 0.06 mg per g of body weight by an intraperitoneal injection.

In Vivo ^{1}H Imaging. Magnetic resonance images were recorded with a 4.7-T Biospec spectrometer (Bruker, Karlsruhe, Germany) equipped with a ^{1}H radio frequency coil of 7.5-cm diameter. The protocol of each experiment included recording of multislice spin echo T_2-weighted images with an echo time (TE) and a repetition time (TR) of 68 and 2400 msec, respectively, accumulating four averages. This was followed by T_1-weighted, spin echo (TE = 15 msec, TR = 400 or 250 msec) images of a selected slice from the center of the tumor, accumulating two averages. After the acquisition of a precontrast T_1-weighted image, a bolus of 0.4 mmol per kg of body weight of N-methylglucamine-GdDTPA (Schering, Berlin) was injected into the tail vein of the mouse. Serial postcontrast T_1-weighted images were then recorded for ≈1 hr with a time resolution of 1.7 or 1.0 min. All images were recorded with a slice thickness of 1 mm and an inplane resolution of 195 μm × 390 μm.

Analysis of the Dynamic Contrast-Enhanced Images. The analysis was based on a model described in detail by Tofts and Kermode (30), which assumes that the contrast agent is distributed in the body as in a multicompartment exchange system. After a bolus injection, a contrast agent such as GdDTPA is rapidly exchanging between the plasma vascular volume and the body extracellular space and is slowly cleared out via the kidneys. The change with time in the concentration of GdDTPA in the plasma was determined from T_1 measurements of blood samples (≈0.5 ml) drawn from injected mice. These T_1 values were converted to concentration units by obtaining a calibration curve of T_1 relaxation versus GdDTPA concentration of plasma samples, to which the contrast agent was added externally. The concentration of GdDTPA in the plasma, $C_p(t)$, assuming that the tumor compartment is small and does not influence the plasma concentration, followed a biexponential decay (30):

$$C_p(t) = D\{a_1\exp(-m_1t) + a_2\exp(-m_2t)\}, \quad [1]$$

where D is the GdDTPA dose of 0.4 mmol per kg of body weight. Fitting the plasma data to Eq. **1** yielded: a_1 = 4.3 kg/liter, a_2 = 3.2 kg/liter, m_1 = 0.43 min^{-1}, and m_2 = 0.057 min^{-1} with a correlation factor, r = 0.976. The amount of GdDTPA in each tumor voxel is $v_1V_tC_1$, where v_1 is the fraction of the voxel which the leakage space occupies, V_t is the voxel volume, and C_1 is GdDTPA concentration in the leakage space. The flow of GdDTPA from the plasma through the permeable capillaries into the free leakage space of a tumor voxel is (30):

$$v_1[dC_1/dt] = (PS/V_t)[(C_p(t) - C_1(t)], \quad [2]$$

where the permeability P(cm·min^{-1}) is defined as the flow of GdDTPA per unit concentration difference across the capillary membrane and per unit surface area (S) of the capillary membrane. The total leakage per voxel is the product $P{\cdot}S$ (cm^3·min^{-1}), and the transfer constant $K = PS/V_t$ (min^{-1}) is termed the permeability factor (30).

The MRI signal enhancement in each voxel depends on the mean concentration of GdDTPA in this voxel ($C_t(t)$) = $v_1C_1(t)$. From the solution to Eq. **2** using Eq. **1** this concentration is (30):

$$C_t(t) = D\{b_1\exp(-m_1t) + b_2\exp(-m_2t) + b_3\exp(-Kt/v_1)\}, \quad [3]$$

where $b_1 = Ka_1/(K/v_1 - m_1)$, $b_2 = Ka_2/(K/v_1 - m_2)$, and $b_3 = b_1 + b_2$.

Signal enhancement in each tumor voxel was determined by calculating $[S(t) - S(0)]/S(0)$, where $S(t)$ and $S(0)$ were the

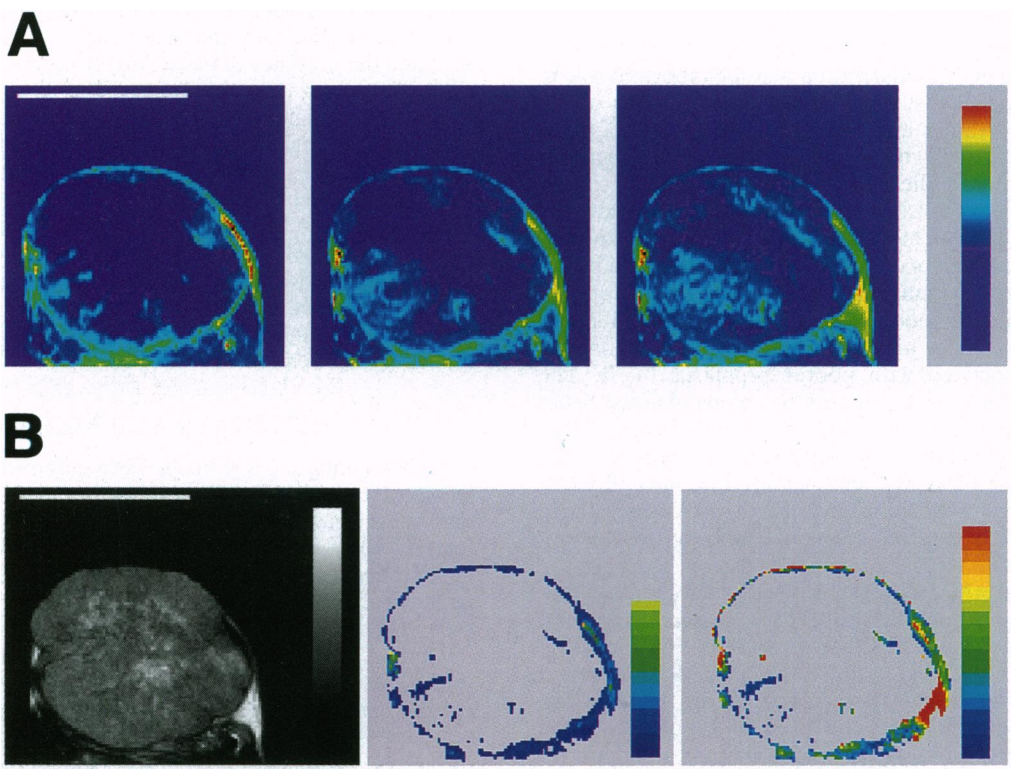

FIG. 1. Contrast-enhanced images of MCF7 tumor grown in the presence of estrogen and image analysis of the dynamic data. (*A*) Spin echo T_1-weighted images (TE/TR = 15/400 msec) recorded in the course of a dynamic contrast-enhanced experiment. Left to right: t = 1.6, 6.6, and 13.3 min after a bolus injection of 0.4 mmol GdDTPA per kg of body weight. Scale bar = 1 cm. (*B*) Left to right: Spin echo T_2-weighted image and maps of permeability factor (K) and of fraction of free leakage space (v_1). The scale of K ranges from 0 to 0.15 min^{-1}, and the scale of v_1 ranges from 0 to 1. Scale bar = 1 cm.

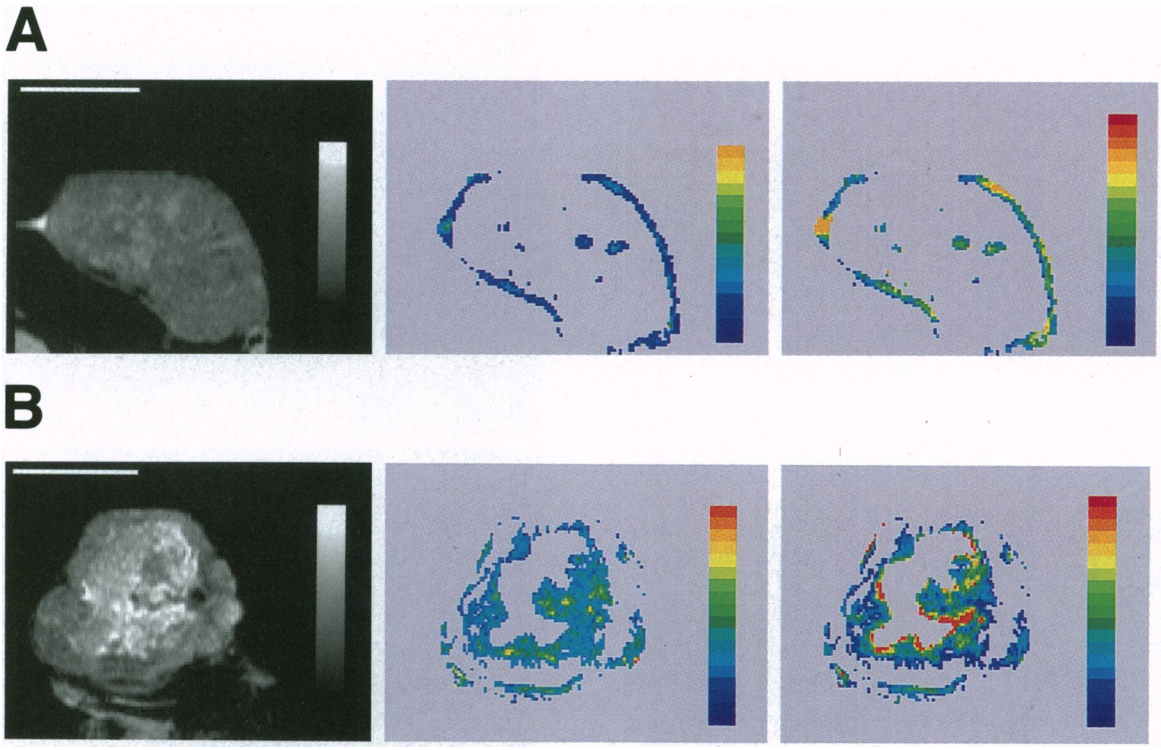

FIG. 2. Spin echo T_2-weighted images and maps of permeability factor (K) and of fraction of free leakage space (v_1) of MCF7 tumors. Left to right: Spin echo T_2-weighted images and maps of permeability factor and of fraction of free leakage space. (*A*) A central slice of a tumor grown in the presence of estrogen. The scale of K ranges from 0 to 0.09 min^{-1} and the scale of v_1 ranges from 0 to 1. Scale bar = 1 cm. (*B*) A central slice of a tamoxifen-treated tumor (3 weeks). The scale of K ranges from 0 to 0.09 min^{-1} and the scale of v_1 ranges from 0 to 1. Scale bar = 1 cm.

measured signal intensities pre- and post-GdDTPA administration, respectively. We have verified that under the applied experimental conditions (the dose of GdDTPA and the MRI spin echo parameters) the enhancement increased linearly with GdDTPA concentration. The variation of signal enhancement with time for a spin echo sequence is:

$$\text{Enhancement}\ (t) = \exp(-R_2C_t(t))\text{TE}$$
$$\{1 - 2\exp[-(\text{TR} - \text{TE}/2)(1/T_{10} + R_1C_t(t))]$$
$$+ \exp[-\text{TR}(1/T_{10} + R_1C_t)\}/$$
$$\{1 - 2\exp[-(\text{TR}-\text{TE}/2)/T_{10}] + \exp(-\text{TR}/T_{10})\} - 1 \quad [4]$$

where R_1 and R_2 are the coefficients for the change in T_1 and T_2 respectively with GdDTPA concentration. Calibration curves at 37°C of T_1 and T_2 versus GdDTPA concentration added to plasma solutions yielded $R_1 = 4.3\ sec^{-1}mM^{-1}$ and $R_2 = 4.9\ sec^{-1}mM^{-1}$. The T_1 value of tumor tissue before GdDTPA injection (T_{10}) was measured independently and was found to be 2.7 ± 0.3 sec. A computer program which fitted the enhancement–time curves per voxel to Eq. **4** with the insertion of $C_t(t)$ according to Eq. **3** yielded the best-fit permeability factor K and fraction of leakage space v_1 for each voxel that exhibited enhancement.

The pattern of contrast distribution with time indicated the presence of two pathways of regional enhancement: rapid enhancement in regions with dense and highly permeable capillaries and slow enhancement, predominantly by diffusion of the contrast agent from the regions with high leakage (see Fig. 1*A*). The slow enhancing regions consisted of tumor tissue with capillaries of low permability or necrotic areas devoid of calillaries. To characterize regions that exhibit highly permeable microvessels, we have selected for the image analysis pixels that exhibited 150% enhancement or more in 5 min (high initial rate of enhancement), which corresponds to a permeability factor >0.01 min^{-1}. All other pixels with either a permeability factor <0.01 min^{-1} or mostly necrotic tissue were excluded.

Histology. Tumors were dissected free from subcutaneous tissue and cut in the middle in the same plane as the images were recorded. The two parts of the tumors were fixed in 4% formaldehyde solution and embedded in paraffin. From each half, several sections of 4-μm thickness were dissected and stained with hematoxylin–eosin and with *Griffonia simplicifolia* lectin, which marks mouse endothelial cells. The details of staining with *Griffonia simplicifolia* lectin were described elsewhere (26).

RESULTS AND DISCUSSION

MCF7 breast tumors grown in the presence of supplemented estrogen reached a size of ≈1 cm^3 within 6 weeks after cell inoculation. MRI images of these tumors were initially recorded using a T_2-weighted spin echo sequence. On the basis of previous correlation studies of MRI and histopathological features (23–27), we have found that these tumors were mostly composed of viable cancer cells with few, scattered, necrotic loci (Fig. 1*B* and Fig. 2*A*). Further dynamic MRI studies with GdDTPA using a T_1-weighted spin echo sequence showed a rapid contrast enhancement in the periphery of the tumors and in several intratumoral regions. The time evolution of contrast enhancement was analyzed as described in *Materials and Methods*, yielding maps of permeability factor and of fraction of leakage space.

Tumors grown in the presence of estrogen (n = 9) showed high permeability factor and high leakage space at the periphery of the tumors (Figs. 1*B*, 2*A* and 3*A*). Part of the peripheral voxels exhibited a rapid initial enhancement, followed by a

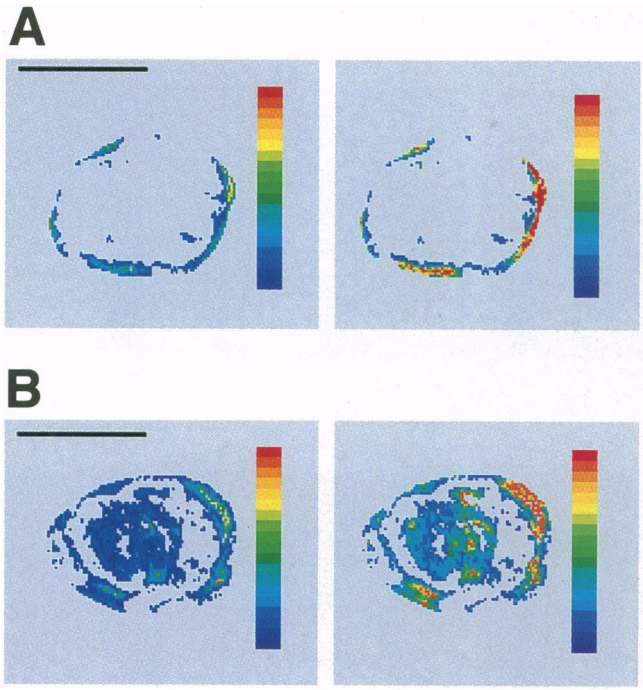

FIG. 3. Maps of permeability factor (K) and of fraction of free leakage space (v_1) of MCF7 tumor before and during tamoxifen treatment. (A) Before tamoxifen treatment. *Left*: Permeability factor; the scale of K ranges from 0 to 0.19 min^{-1}. *Right*: Fraction of leakage space; the scale of v_1 ranges from 0 to 1. Scale bar = 1 cm. (B) Thirteen days of tamoxifen treatment. *Left*: Permeability factor; the scale of K ranges from 0 to 0.25 min^{-1}. *Right*: Fraction of leakage space; the scale of v_1 ranges from 0 to 1. Scale bar = 1 cm.

decay similar to that found in the plasma, with leakage space close to 1. These voxels may contain large vessels of a voxel dimension. Inspection of the tumors before dissection confirmed the presence of visible vessels around the tumors margin. The remaining peripheral voxels exhibited enhancement curves, indicating leakage from microvessels. Such peripheral microcapillaries were observed in the histological sections.

The presence of intratumoral leaky microcapillaries in estrogen-supplemented tumors was relatively scarce (Figs. 1*B*, 2*A*, and 3*A*) despite the network of microcapillaries demonstrated by the endothelial cell staining (Fig. 4*A*), as reported (26). The high cellularity and continuous growth of these tumors require the presence of microcapillaries that deliver nutrients and oxygen and clear out waste products. We have therefore concluded that most of the microcapillaries in the cellular regions of MCF7 tumors behave like most microcapillaries of healthy tissues, which exhibit low permeability to GdDTPA. As in normal tissues, no substantial enhancement due to the presence of GdDTPA inside these intact microcapillaries could be detected in images recorded with a voxel size, which was large compared to the net volume of the capillaries. On the other hand, in voxels with, or close to, permeable capillaries the rapid leakage of GdDTPA into an interstitial space that occupied most frequently >20% of a voxel volume led to a visible, significant enhancement.

As described above, the estrogen-treated tumors were highly cellular, but part of these tumors contained scattered necrotic loci (Figs. 1*B* and 2*A*). In these tumors, the derived permeability maps indicated the presence of regions with high permeability factor and high leakage space in the vicinity of the necrotic loci. The display of intratumoral, highly leaky vessels at the boundaries of necrotic regions was even more pronounced in tamoxifen-treated MCF7 tumors (n = 8; Figs. 2*B* and 3*B*). Previous MRI studies of MCF7 tumors in our

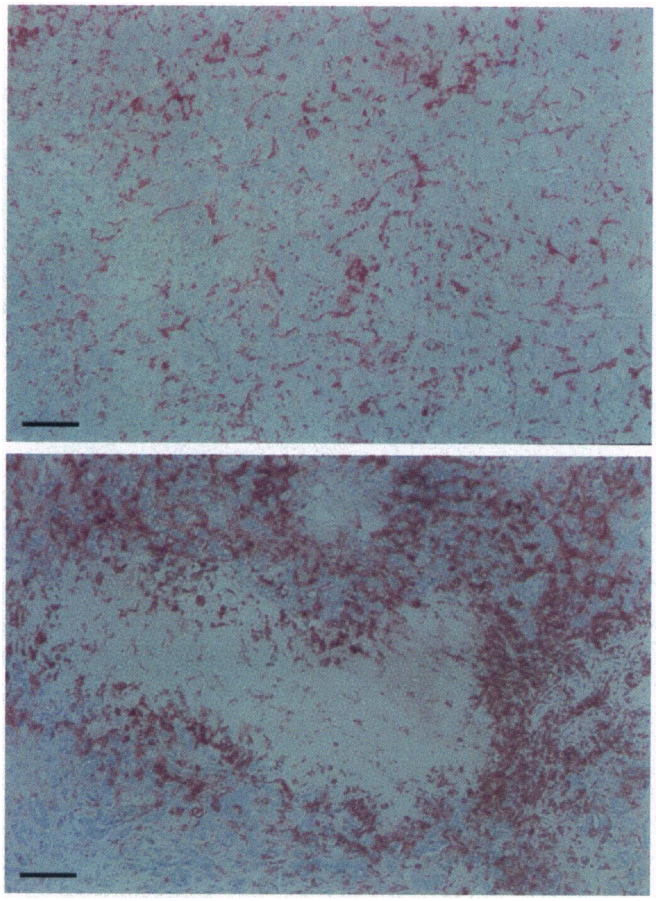

FIG. 4. Microscopic view of endothelial cells in histological sections of MCF7 tumors stained with *Griffonia simplicifolia* lectin. (A) Endothelial cells in a viable cellular area of a tumor grown in the presence of estrogen. (B) Endothelial cells localized at the boundary of necrosis in a tumor treated with tamoxifen for 2 weeks. The scale bar indicates 30 μm. The details of the staining procedure were described in ref. 26.

laboratory have demonstrated rapid development of central necrosis as a result of tamoxifen treatment (23–27). In regions surrounding these necrotic areas, a marked increase in the rate of GdDTPA enhancement was observed. Permeability maps derived from dynamic studies delineated the high permeability factor in these boundary zones (Fig. 2*B*). Permeability factor and leakage space maps of tumors studied before and during tamoxifen treatment (Fig. 3) showed clearly a marked outgrowth of intratumoral permeable capillaries around necrotic areas, developed as a result of the treatment. This localized angiogenic stimulation was further confirmed by immunostaining of endothelial cells. High density of endothelium at regions surrounding necrotic loci were observed in tamoxifen-treated tumors (Fig. 4*B*), as well as in estrogen-treated tumors that exhibited significant necrosis. It is important to note that while histology showed the presence of dense endothelial cells in the immediate vicinity of necrotic areas, the maps derived from the MRI data showed that these endothelial cells form highly permeable microcapillaries.

The presence of dense and highly permeable capillaries in regions bordering necrosis indicates induction of angiogenesis in the vicinity of regions experiencing stress conditions that lead to cell death. Stress conditions such as hypoxia and ischemia were shown to evoke overexpression of mRNA of VEGF/VPF in tumor cells that were adjacent to zones of necrosis (28, 29). This presence of overexpression of VEGF/VPF and the finding of highly permeable vessels at the boundary of necrotic locations appear to be associated with the

same stimulation. Recent studies of MCF7 tumors showed up-regulation of VEGF/VPF in regions that also exhibited high permeability factor and were localized in the boundary of necrotic areas (E.F.-H., A. Itin, E. Keshet, and H.D., unpublished data). We therefore propose that regions adjacent to necrosis, which show rapid contrast enhancement due to the presence of leaky vessels, might exhibit up-regulation of VEGF/VPF.

It was previously shown that microvessel density in areas of most intense neovascularization ("hot spots") is an independent and highly significant prognostic indicator for overall relapse free survival in patients with early stage breast carcinoma (5). The neovascular hot spots were found to occur most frequently at the periphery of the carcinoma (5, 31). In MCF7 tumors, regions that exhibited contrast enhancement due to the presence of dense and leaky capillaries were found in the periphery of the tumors and in the vicinity of intratumoral necrotic regions. Whether these capillaries are the ones used by immunostaining to assess patients prognosis is not known, but further correlation studies between contrast-enhanced MRI of breast cancer patients and immunostaining of microcapillaries may resolve this question.

To summarize, we have analyzed the variation with time in GdDTPA enhancement of MCF7 tumors. A detailed image analysis yielded maps of microcapillary permeability times surface area and of fraction of interstitial leakage space. These maps and correlation with histochemical studies confirmed the presence of dense microvessels at the tumor peripheral areas and at the vicinity of intratumoral necrotic regions. Most of the enhancement in the MRI resulted from the fast leakage from these permeable microcapillaries. On the basis of these results we propose stress-induced angiogenesis as one of the main mechanisms responsible for the observed contrast enhancement in MRI of breast carcinoma and possibly in other types of malignancies. The distribution and extent of this angiogenic activity derived from dynamic GdDTPA-enhanced MRI may serve to increase the specificity of breast cancer diagnosis and predict prognosis.

We would like to thank Dr. Ada Horowitz and Dr. Iris Goldberg from the Department of Pathology at the Sheba Medical Center for their assistance in the course of this work. This work was supported by the National Cancer Institute Grant CA42238.

1. Folkman, J. (1985) *Adv. Cancer Res.* **43,** 175–203.
2. Folkman, J. (1995) *Nat. Med.* **1,** 27–31.
3. Holmgren, L., O'Reilly, M. S. & Folkman, J. (1995) *Nat. Med.* **1,** 149–153.
4. Weidner, N., Semple, J. P., Welch, W. R. & Folkman, J. (1991) *N. Engl. J. Med.* **324,** 1–8.
5. Weidner, N., Folkman, J., Pozza, F., Bevilacqua, P., Allred, E. N., Moore, D. H., Meli, S. & Gasparini, G. (1992) *J. Natl. Cancer Inst.* **84,** 1875–1887.
6. Horak, E. R., Leek, R., Klenk, N., Lejeune, S., Smith, K., Greenall, N. S., Stepniewska, K. & Harris, A. L. (1992) *Lancet* **340,** 1120–1124.
7. Bosari, S., Lee, A. K., DeLellis, R. A., Wiley, B. D., Heatley, G. J. & Silverman, M. L. (1992) *Hum. Pathol.* **23,** 755–761.
8. Macchiarini, P., Fontanini, G., Hardin, M. J., Squartini, F. & Angeiletti, C. A. (1992) *Lancet* **340,** 145–146.
9. Weidner, N. (1994) *Semin. Diagn. Pathol.* **10,** 302–313.
10. Weidner, N., Carroil, P. R., Flax, J., Blumenfeld, W. & Folkman, J. (1993) *Am. J. Pathol.* **143,** 401–409.
11. Vaupel, P., Kallinowski, F. & Okunieff, P. (1989) *Cancer Res.* **49,** 6449–6465.
12. Jain, R. K. (1988) *Cancer Res.* **48,** 2641–2658.
13. Heywang-Kobrunner, S. H. (1994) *Invest. Radiol.* **29,** 94–104.
14. Kaiser, W. A. & Zeitler, E. (1989) *Radiology* **170,** 681–686.
15. Kennedy, SD, Szczepaniak, L. S., Gibson, S. L., Hilf, R., Foster, T. H. & Bryant, R. G. (1994) *Magn. Reson. Med.* **31,** 292–301.
16. Hanna, S. L., Reddick, W. E., Parham, D. M., Gronemeyer, S. A., Taylor, J. S. & Fletcher, B. D. (1993) *J. Magn. Reson. Imag.* **3,** 849–853.
17. Gowland, P., Mansfield, P., Bullock, P., Stehling, M., Worthington, B. & Firth, J. (1992) *Magn. Reson. Med.* **26,** 241–258.
18. Larsson, H. B. W., Stubgaard, M., Frederiksen, J. L., Jensen, M., Henriksen, O. & Paulson, O. B. (1990) *Magn. Reson. Med.* **16,** 117–131.
19. Brix, G., Semmler, W., Port, R., Schad, L. R., Layer, G. & Lorenz, W. J. (1991) *J. Comput. Assist. Tomogr.* **15,** 621–628.
20. Su, M.-Y., Jao, J.-C. & Nalcioglu O. (1994) *Magn. Reson. Med.* **32,** 714–724.
21. Hoffmann, U., Brix, G., Knopp, M. V., Hess, T. & Lorenz, W. J. (1995) *Magn. Reson. Med.* **33,** 506–514.
22. Tofts, P. S., Berkowitz, B. & Schnall, M. D. (1995) *Magn. Reson. Med.* **33,** 564–568.
23. Furman, E., Margalit, R., Bendel, P., Horowitz, A. & Degani, H. (1991) *Cancer Commun.* **3,** 287–297.
24. Furman, E., Rushkin, E., Margalit, R., Bendel, P. & Degani, H. (1992) *J. Steroid Biochem. Mol. Biol.* **43,** 189–195.
25. Degani, H., Furman, E. & Fields, S. (1994) *Clin. Chim. Acta* **228,** 19–33.
26. Haran, E. F., Maretzek, A. F., Goldberg, I., Horowitz, A. & Degani, H. (1994) *Cancer Res.* **54,** 5511–5514.
27. Furman-Haran, E., Margalit, R., Maretzek, A. F. & Degani, H. (1996) *J. Magn. Reson. Imag.* **6,** 195–202.
28. Shweiki, D., Itin, A., Soffer, D. & Keshet, E. (1992) *Nature (London)* **359,** 843–845.
29. Brown, L. F., Berse, B., Jackman, R. W., Tognazzi, K., Manseau, E. J., Senger, D. R. & Dvorak, H. F. (1993) *Cancer Res.* **53,** 4727–4735.
30. Tofts, P. S. & Kermode, A. G. (1991) *Magn. Reson. Med.* **17,** 357–367.
31. Vartanian, R. K. & Weidner, N. (1994) *Am. J. Pathol.* **144,** 1188–1194.